IEEE Access
Multidisciplinary | Rapid Review | Open Access Journal

Received April 24, 2019, accepted May 30, 2019, date of publication June 5, 2019, date of current version June 20, 2019.

Digital Object Identifier 10.1109/ACCESS.2019.2921288

Hard X-Ray Emission Detection Using Deep Learning Analysis of the Radiated UHF Electromagnetic Signal From a Plasma Focus Discharge

GONZALO AVARIA[1,3], JORGE ARDILA-REY[2], SERGIO DAVIS[1,3], LUIS ORELLANA[2], BENJAMÍN CEVALLOS[2], CRISTIAN PAVEZ[1,3], AND LEOPOLDO SOTO[1,3]

[1]Departamento de Ciencias Nucleares, Comisión Chilena de Energía Nuclear, Casilla 188-D, Santiago 7600713, Chile
[2]Department of Electrical Engineering, Federico Santa Maria Technical University, Santiago 8940000, Chile
[3]Departamento de Ciencias Físicas, Facultad de Ciencias Exactas, Universidad Andres Bello, Republica 220, Santiago 8370035, Chile

Corresponding author: Gonzalo Avaria (gonzalo.avaria@cchen.cl)

This work was supported by in part by the Fondecyt Iniciación under Grant 11160115 and in part by the "Dirección de Postgrados y Programas" of Universidad Técnica Federico Santa María under PIIC grant.

ABSTRACT A method to determine the presence of hard X-ray emission processes from a dense plasma focus (205 J, 22 kV, 6.5 mbar H_2) using Ultra High Frequency (UHF) measurements and deep learning techniques is presented. Simultaneously, the electromagnetic UHF radiation emitted from the plasma focus was measured with a Vivaldi UHF antenna, while the hard X-ray emission was measured with a scintillator-photomultiplier system. A classification algorithm based on deep learning methods, using two-dimensional convolutional layers, was implemented to predict the hard X-ray signal standard deviation value using only the antenna signal measurement. Two independent datasets, consisting of 999 and 1761 data pairs each, were used in the analysis. Different realizations of the training/validation process using a deep learning model, obtained overall better results in comparison to other machine learning methods like k-neighbors, decision trees, gradient boost, and random forest. The results of the deep learning algorithm, and even its comparison with other machine learning methods, indicate that a relationship between the electromagnetic UHF radiation and hard X-ray emission can be established, enabling the indirect detection of hard X-ray pulses only using the UHF antenna signal. This indirect detection presents the opportunity to have a simple and low-cost diagnostic, compared to the methods currently used to characterize the pulses of X-rays emitted from plasma focus discharges.

INDEX TERMS Deep learning, Plasma focus, UHF antenna, X-ray pulse.

I. INTRODUCTION

Pulsed discharges have the capability to produce pulses of electromagnetic radiation, charged and neutral particles. These plasma devices have many configurations. One of them is the Z-pinch [1], which comprises different architectures such as wire arrays [2], capillary discharges [3], X-pinch [4], gas embedded Z-pinch [5] and Plasma Focus (DPF) [6], amongst others. The latter has seen a renewed interest from the international plasma community due to its many interesting capabilities: as a portable pulsed neutron source for field applications [7]–[10], as a pulsed X-ray source [11], as an ion beam accelerator [12], to produce plasma shocks [13], to produce supersonic plasma jets of astrophysical interest [14], to test new materials for the first wall in fusion reactors [15], to synthesize new materials and nanomaterials [16], [17], and also as a pulsed neutron source for cancerous cell irradiation [18].

The Dense Plasma Focus (DPF) device consists of a set of capacitors, a high voltage spark gap and concentric electrodes separated by an insulating sleeve. Hydrogen (or deuterium or other gases) at a low pressure (few mbar) is injected in a vacuum chamber surrounding the electrodes. Once the capacitors are charged to voltages in the order of tens of kV, the spark gap is triggered and a plasma sheath is formed

The associate editor coordinating the review of this manuscript and approving it for publication was Malik Jahan Khan.

above the insulating sleeve. The dynamics of the plasma discharge are divided into six stages [6]: I) breakdown, when a current sheath is formed on the surface of the insulator; II) axial acceleration, when the plasma sheath separates from the insulator and is accelerated towards the end of the concentric electrodes; III) radial acceleration, when the plasma sheath reaches the top of the electrodes, the magnetic fields created by the electron current accelerates the plasma sheath towards the center of the anode; IV) pinch, when the radial phase reaches an stagnation point, the plasma reaches a high temperature and density [19]; V) plasma shock, after the pinch disruption [13]; VI) plasma jet, after the plasma shock advances away from the electrode, plasma jets are ejected [14].

During the pinch phase, high intensity electric fields are generated in the plasma column, producing conditions that accelerate electrons towards the anode [20]. The interaction of this electron beam with the anode surface enables the generation of intense hard X-ray pulses [20]–[23], which can be detected with scintillator-photomultiplier systems [6], [24]–[28], radiographic film [11], pinhole photography and semiconductor detectors [27], [28], amongst other methods [20], [26].

In parallel to the high energy radiation generated by these devices, emission in the Ultra High Frequency (UHF) range has also been detected and associated to induced damage in electronic circuits through coupling of the high frequency electric field with instrument cables [29]. In order to characterize these electromagnetic transients, antennas with high efficiency and directivity are paramount due to their excellent performance. High efficiency is mainly achieved by minimizing reflection losses with an appropriate geometry, i.e. tunning the antenna for a particular frequency band [30]. On the other hand, directivity accounts for the maximum radiation intensity in a particular direction which is also determined by the design of the antenna [30]. For example, the Vivaldi antenna is a planar antenna characterized by an exponential slot line embedded in dielectric substrate and it is feeded with a microstrip transmission line [31]. This particular design allows the measurement of a wide frequency band instead of just particular resonant frequencies, detected when using dipole or monopole antennas. This type of antenna had been used for measuring electrical disruptions in insulation systems (partial discharges), which also emits a fast EM transient in the VHF/UHF frequency range [32].

Different antenna designs have been used in Plasma Focus devices, in order to obtain information about plasma dynamics and physical processes happening in the discharge. For example, Schmidt et al. [33] used a monopole antenna placed inside the vacuum chamber and compared the measured signal with simulated electric field oscillations (E_z), relating the high frequency content (up to 5 GHz) emission to good neutron yield pinches. Horn antennas with a highly directional radiation pattern and tuned for the microwave range of frequencies, in combination with waveguides and microwave crystal detectors, were used as a time of flight spectrometer for the radiation emitted on the outside from a DPF [34]. A dipole antenna, which has an omni-directional radiation pattern and is tuned for a particular frequency, was used on the outside of the vacuum chamber in order to measure the electromagnetic burst from a DPF device [29]. Except for the papers of Gerdin *et al.* [34] and Schmidt *et al.* [33], no further relationship of the EM radiation with plasma focus phenomena has been reported. Using a Mirnov Coil, an inductive sensor, Piriaei *et al.* [35] associated a relation between the measured signal and changes in the electrode geometry of a plasma focus device.

Signals obtained from electromagnetic radiation sensors have different frequency contents, ranging from MHz to GHz, which makes the analysis of this information a very complex procedure. In order to obtain statistically meaningful observations, a large dataset size is required, as well as the possibility to adequately characterize the signals in the different dimensions that it can be described. Considering the complexity of the EM signals, as well as the large amount of data acquired, the use of artificial intelligence algorithms is crucial to be able to determine information hidden in those signals. There has been a resurgence in the area of machine learning due to the success of the so-called deep learning approach [36], with remarkable applications in computer vision [37], natural language processing [38], audio synthesis and recognition [39], strategy games such as Go and chess [40], [41] and recently, in different areas of plasma physics [42] and controlled fusion plasmas [43], among many others.

This work presents a novel technique to identify highly transient phenomena that produces exceptional conditions in the pulsed plasma column, capable to efficiently generate hard X-ray emission, using the radiated EM signal measured with a Vivaldi antenna and analyzed with deep learning algorithms.

II. METHODOLOGY

A. PLASMA FOCUS DISCHARGE

Measurements of the UHF signal and hard X-ray emission were performed at the PF-400J [7] discharge. The discharge was operated at $\sim$ 205 J stored energy (22kV charging voltage, $\sim$ 332 ns quarter period) with a modified electrode geometry. The insulator had an effective length of 21.5 mm (from the top of the cathode plate edge) and the stainless steel anode had a $z_{eff} = 13\ mm$. Return rods were removed in this configuration. A very high rate of shots with axial hard X-ray emission was obtained with these modifications: more than 75% of shots had a distinguishable hard X-ray signal on the photomultiplier. The discharge was operated in pure Hydrogen at a pressure of 6.5 mbar. A schematic drawing of the experimental setup can be seen in Fig. 1.

The detection of the hard X-ray emission from the discharges was done with a scintillator-photomultiplier tube (PMT) system, located axially above at 0.54 m from the anode. The PMT (Hamamatsu R1828-01) produces an electrical signal proportional to the amount of incident light. Simultaneously, the UHF/VHF electromagnetic

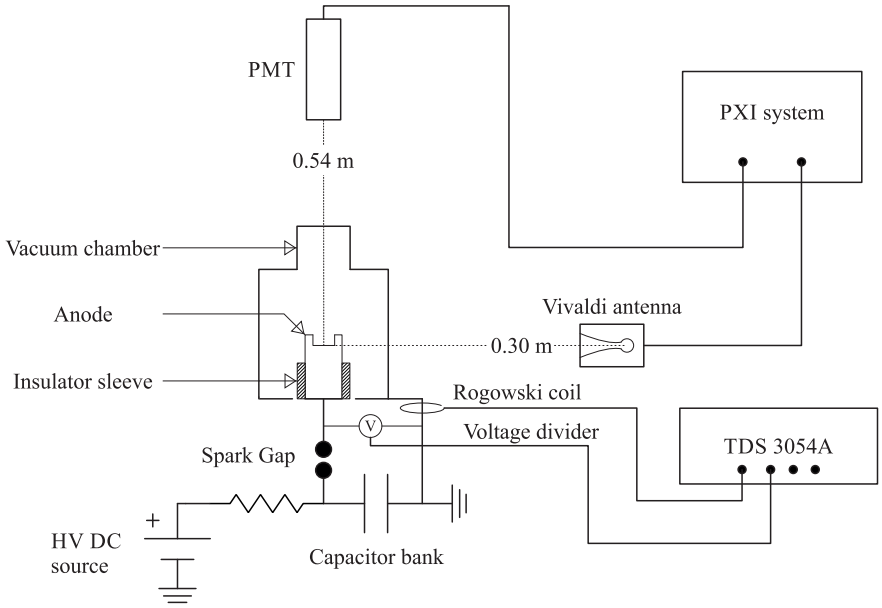

FIGURE 1. Schematic of the experimental configuration of the experiment.

emission was measured using a Vivaldi antenna placed 0.30 m radially from the anode center. These two signals were acquired, digitized and processed by a PXI system, which is composed by a NI-PXIe-1082 chassis, an NI-PXI 5162 acquisition card (with sampling frequency of 12.5 GS/s, 8 bits of vertical resolution and 3 GHz of bandwidth with a 50 Ω input), and a NI-PXIe-8115 controller with a dual-core i5-2510E processor. This system was configured to acquire each of the signals, X-ray emission and EM radiation, with a sampling frequency of 6.25 GS/s and a time window of 0.9 μs.

To avoid any over-voltage in the input channels of the measurement system, commercial attenuators were used. These devices had 20 and 30 dB attenuation with bandwidths between 0-18 GHz and 0-6 GHz respectively.

Conventional electric signal diagnostics were used in order to monitor the DPF device operation. A Rogowski coil, widely used to characterize the current derivative signal [44], was coupled to the current return path of the device. A resistive voltage divider, commonly used for measuring high voltage impulses [45], was placed between the anode terminal and ground. These signals were acquired with a Tektronik TDS 3054A oscilloscope (4 channels, 5Gs/s and 300 MHz bandwidth).

B. VIVALDI ANTENNA

Instrumentally, an antenna can be considered as a transducer capable of bidirectionally converting any electromagnetic signal into an electrical signal [30]. In practical terms, for an antenna to properly measure the electromagnetic emission from the high-energy transients that are generated from DPF devices, the maximum values of the radiation pattern of both the emission of the transient and the reception of the antenna must coincide. That is to say, the antenna radiation pattern must be oriented towards the source of the transient so that the electric and magnetic fields that are being captured generate the highest possible voltage at the terminals of the antenna and, consequently, receive a higher energy value [46], [47]. Due to the pulsing behavior of DPFs, some spectral components of the transients, generated during their operation, can appear in frequency bands where there are permanently-present spectral contents associated with electromagnetic noise: FM radio, digital TV, Digital Audio Broadcasting (DAB), Global System for Mobile communications (GSM) and Wi-Fi [29], [48]. For this reason, the antenna must be adjusted or calibrated so that it can measure the bands where this noise is not present, and thus, the information captured would correspond as much as possible to the pulse that is being measured. The Vivaldi antenna stands out among the possible antennas that can be used in the measurement and characterization of pulses that come from DPFs, as it can be adjusted geometrically so that it omits frequency bands where the electromagnetic noise is of great amplitude. According to its waveguide design, the Vivaldi antenna is very directional, which is an advantage, since it minimizes the measurement of external sources to the area where the antenna is directed. Moreover, its simple construction and low cost make this antenna of great interest for these types of applications [32], [49]. The Vivaldi antenna that was used for the experimental measurements of the present work was constructed from a circuit board, where the total surface of the antenna measured 8.5 cm x 11.3 cm, with a thickness of 1.3 mm in the dielectric substrate that is located between the conductive faces of the plate. Fig. 2 shows the Vivaldi antenna implemented, together with its corresponding parameter S_{11}.

Fig. 2b shows the parameter S11, which was obtained from a MS2035B network analyzer. This parameter is considered

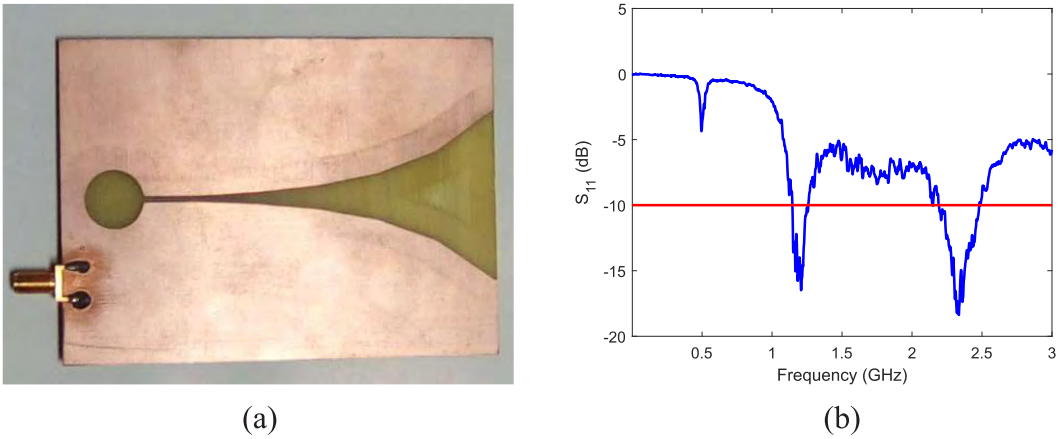

FIGURE 2. Vivaldi antenna (a) and its S_{11} parameter (b).

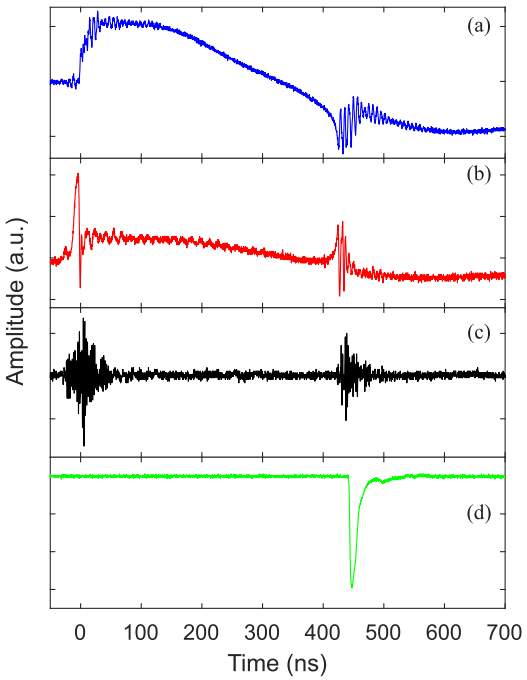

FIGURE 3. Typical measurement waveforms (data taken with the TDS oscilloscope): (a) Discharge di/dt signal from Rogowski coil, (b) Voltage divider signal, (c) Vivaldi antenna signal and (d) photomultiplier signal.

as a reference measure, since it represents the frequencies to which the antenna is tuned and is key for determining its efficiency at each of the operating frequencies. According to what is shown in Fig. 2b, the S11 value of 0 dB indicates a reflection of 100% of the signal, while that of 10 dB indicates a power reflection of 10%. Based on the topology and the dimensions used, the Vivaldi antenna was adapted for the frequency bands where the losses by reflection were less than 10 dB, i.e. 1.25 GHz and 2.4 GHz. This configuration is adequate, since it omits the noise sources associated with FM radio, DAB and part of the band corresponding to GSM during the measurement, which have more energy in the electromagnetic spectrum of up to 3 GHz. However, it should be noted that the antenna can also measure in the rest of frequency bands with a greater or lesser degree of attenuation according to what the parameter S_{11} indicates.

III. RESULTS

An example of the electrical signals from a pulsed plasma focus discharge, with high x-ray emission, are shown in Fig. 3. A high frequency event is seen at $t \approx 425$ ns, which is associated with the pinch (column compression due to high intensity magnetic fields), and is detected by all the sensors. Signals from conventional electrical sensors used for DPF characterization [20], such as a Rogoswki coil and a voltage divider, can be seen in Fig. 3a and 3b, respectively. Vivaldi antenna and photomultiplier (PMT) signals, from the same discharge, are shown in Fig. 3c and 3d. The deep learning algorithm was fed with data pairs consisting of antenna and PMT signals for each shot.

From the naked eye observation of the antenna signal, it is evident that its complexity makes the identification of shots with hard X-ray emission, an impossible task. For example, Fig. 4 shows two different antenna signals from different discharges, which have notorious amplitude differences. At the pinch moment, the amplitude of the signals is dramatically different. Nevertheless, both of them had a high hard X-ray emission. On the contrary, Fig. 5 shows very similar antenna signals, although Fig. 5a has X-ray emission while 5b is lacking such emission. As seen in this comparison of the antenna signals, it is clear that a more complex analysis tool is needed to determine if the EM emission contains information about the physical processes that generate the conditions for hard X-ray emission from the pulsed discharge. Machine learning algorithms have the capability to identify patterns in complex signals, which enables the search for a relation between the EM and hard X-ray emission.

Considering that the machine learning analysis could be influenced by over-fitting, due to the complexity of the signals that are fed to the algorithm, a discretization of the intensity values of the hard X-ray PMT signal was used.

In this case, to obtain a measure of the intensity of the hard X-ray emission pulse, a discrete version of the root mean

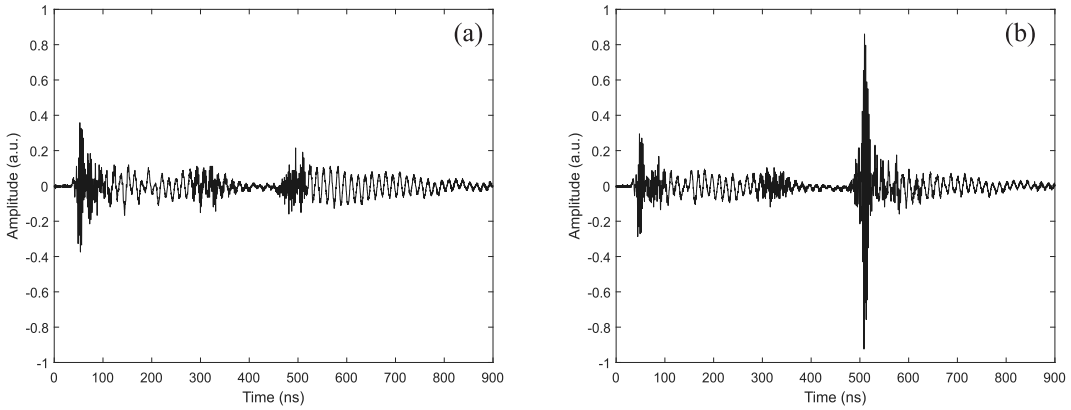

FIGURE 4. Different Vivaldi antenna waveforms that yielded notorious X-ray signals: (a) small amplitude oscillations and (b) high amplitude oscillations seen at the pinch moment.

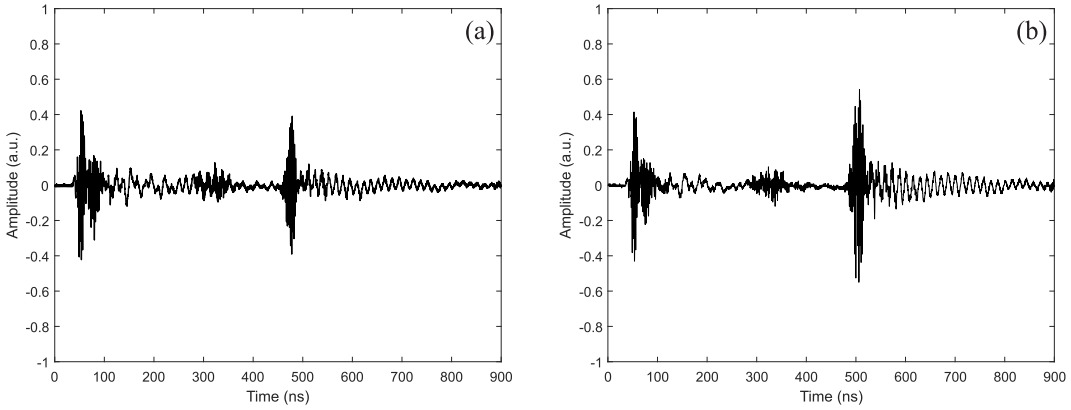

FIGURE 5. Similar Vivaldi antenna waveforms: (a) signal associated with X-ray emission and (b) signal associated with no X-ray emission.

square (RMS) of the photomultiplier signal –essentially given by its standard deviation– was used. It can be represented by

$$S = \sqrt{\frac{1}{N-1}\sum_{i=1}^{N}(f_i - \overline{f})^2}, \tag{1}$$

where $\overline{f}$ is the average of the photomultiplier signal,

$$\overline{f} = \frac{1}{N}\sum_{i=1}^{N} f_i. \tag{2}$$

The base level $S_{\text{ref}} = 2.0185 \times 10^{-4}$, corresponding to the background without emission, was used as a reference in order to report a normalized quantity $R = S/S_{\text{ref}}$, such that $R \geqslant 1$. Using the value of R, four categories were defined and are shown in Table 1. Observed frequency corresponds to the percentage of shots that fulfills a particular category in relation to the total number of shots. The range of values for R was selected to have categories with a similar value of the Observed Frequency, avoiding a bias towards a particular one. In terms of a binary classification problem, these categories can be reduced to merely distinguishing between A and not A.

TABLE 1. Four categories of intensity of emission of hard X-rays, according to the normalized RMS index R.

Label	Description	Range	Observed frequency
A	No emission	$R < 1.1$	14.8%
B	Low emission	$1.1 \leq R < 2$	29.7%
C	Medium emission	$2 \leq R < 10$	22.7%
D	High emission	$R \geq 10$	32.8%

It is important to note that no preprocessing of the antenna signal was performed in terms of frequencies, only its mean value was substracted and the global scale was fixed so that the standard deviation of the input signal is always 0.045. This value was chosen so that the antenna signal values are always between -1 and 1, as a form of regularization for the neural network.

The datasets considered for the machine learning algorithm are shown in Table 2. Dataset 1 corresponds to the first measurement campaign, two separate days, intended to test if the deep learning algorithm could detect any relationship between the signals. Dataset 2 was acquired in a different campaign, to give more variability and test the generalization of the algorithm using independent experimental data.

A bidimensional convolutional neural network (CNN) categorical classifier was constructed in order to analyze the

TABLE 2. Experimental datasets used in the machine learning algorithm.

	Dataset 1	Dataset 2
Number of Vivaldi/PMT signal pairs	999	1761

data. This was done by stacking three convolutional layers, each of them followed by a dropout layer (which helps reduce overfitting) and a max pooling layer, as shown in Fig. 6. The antenna signal was used as input, padded to form a vector of length $5625 = 75 \times 75$, and a categorical output was obtained using the softmax activation function, as usual. In summary, the whole neural network works as a nonlinear function which is able to map the 2D representation of the antenna signal into a category according to the standard deviation value of the associated PMT signal, as shown in Table 1. The algorithm was entirely implemented using the Keras [50] framework with a TensorFlow backend. The CNN reported in this paper corresponded to the architecture that gave better results according to the initial survey using dataset 1. During the preliminary tests, several neural network and training parameters were varied in order to avoid overfitting and improve convergence. For instance, the `RMSProp` and `Adam` optimizers were used, and their learning rates were changed from their Keras default values of 0.001 in the range (0.01, 0.0001). Regarding the activation functions, we tested the performance of `sigmoid`, `tanh` and `relu` for binary classification, finally choosing for the latest, and also chose `softmax` for multi-class classification, as is standard. In all these tests we only noticed differences regarding the rate of convergence (number of epochs needed to reach a certain level of validation accuracy), while the success of the learning process was strongly determined by the size of the neural networks and the presence and values of the *dropout* layers. No modifications of the architecture (number of layers, activation functions, etc.) were attempted for dataset 2.

For the first analysis, dataset 1 and 200 data pairs from one measurement instance of dataset 2 were used. The training process was performed using 799 samples (corresponding to 80 percent of the 999 samples available) as training data, and the remaining 200 samples as testing data. An example of the evolution of a single neural net during the training process is shown in Fig. 7. Here we see that, in terms of both accuracy and loss is clear that a certain amount of overfitting occurs (because the validation accuracy lags slightly behind the training accuracy, while the validation loss remains above the training loss).

A group of 200 data pairs, not used before, were considered for performance evaluation of this first model against new data. The results obtained for categorical classification are shown in Table 3. In this case, full identification means the neural network correctly predicts the category, while partial identification means the neural network only correctly predicts the presence or absence of emission (i.e. if the category is A or not).

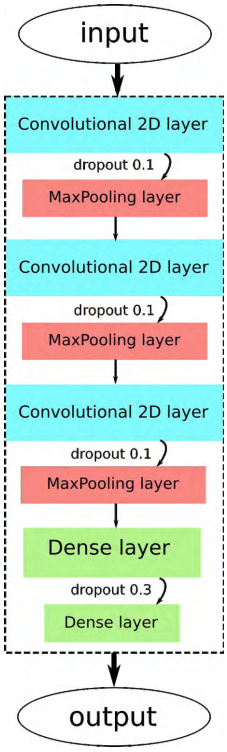

FIGURE 6. Architecture of the convolutional neural network.

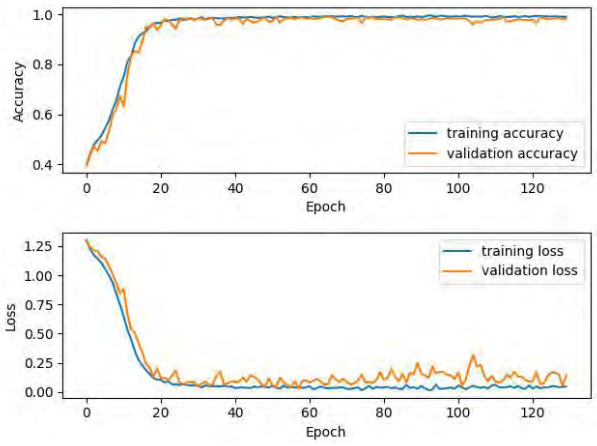

FIGURE 7. Training metrics (including cross-validation).

It should be noted that despite the fact that the rate for full identification is below 50%, it is far above the performance of random guessing, which in this case is one out of four, or 25%. In fact, the probability of obtaining this outcome (92 correct guesses out of 200) by mere chance is given by a binomial distribution (3) with $p = 1/4$,

$$P(k = 92|n = 200, p = 0.25) = \binom{200}{92}\left(\frac{1}{4}\right)^{92}\left(\frac{3}{4}\right)^{108} = 6.268 \times 10^{-11}. \quad (3)$$

As only reporting accuracy (percentage of correct cases over total cases) may be misleading in the case when the frequencies in the training/validation set are highly biased,

TABLE 3. Results for categorical classification.

Result	Cases	Percentage
Full identification	92 out of 200	46%
Partial identification	79 out of 200	39.5%
False positive	23 out of 200	11.5%
False negative	6 out of 200	3%

TABLE 4. Results of several metrics used for binary classification for the CNN algorithm. Statistics were collected over 40 realizations of the training process.

Metric	Dataset 1	Dataset 2
Accuracy	86.5 ± 2.2	87.7 ± 1.5
Precision	87.9 ± 2.7	87.9 ± 1.5
Recall	97.7 ± 1.9	99.6 ± 0.5
Specificity	22.2 ± 14.1	2.3 ± 3.1
F_1 score	92.5 ± 1.3	93.4 ± 0.9

we report the results for binary classification (category A or not A) in terms of several, complementary diagnostics, namely precision, recall, specificity and F_1 score. For this binary classification analysis both datasets were used. In particular, for each dataset, 80% of the available samples were used for training and the remaining 20% for validation. Furthermore, the training/validation process was carried out 40 times, using randomly selected signals for training/validation, to take into account the precision and dispersion of the results for each metric. The binary classification results are shown in Table 4. Complementary diagnostics are described as follows: *accuracy* is simply the fraction of correctly classified samples over the total number of samples; *precision* is the fraction of true positives (in our case, real hard X-ray emission) over the number of announced positives; *recall* is the fraction of correctly detected positives over all existing positive samples, while *specificity* is the fraction of correctly detected negative samples (real absence of hard X-ray emission) over all existing negative samples. From these diagnostics the F_1 score can be computed as the harmonic average between precision and recall. More details of these metrics are found elsewhere [51].

From Table 4 it is shown that the F_1 score gives a reasonable performance for the hard X-ray emission identification, and by extension precision and recall, while the low value of specificity is consistent with the fact that in our case most of the misclassifications are false negatives.

Considering the results shown in Table 3 and the metrics defined in Table 4, a definitive relation can be inferred between the emitted EM signal and the hard X-ray emission from a pulsed plasma device. In some cases the algorithm could even predict a range for the standard deviation value associated with a certain PMT signal. These results are reinforced by a comparison with several machine learning algorithms, shown in Table 5. We can see that all algorithms are able to capture the correlation between the signals, to some degree. As expected, the traditional algorithms such as k-neighbors and decision trees do not perform as well as the newer ensemble methods such as gradient boosting and random forests, while the CNN gives an additional performance increase over all of them.

TABLE 5. Results of several metrics in binary classification for some traditional machine learning algorithms, using the dataset 2. Statistics were collected over 40 realizations of the training process. First column indicates the metric used for the comparison, as seen in Table 4.

	k-Neighbors	Decision trees	Gradient boost	Random forest
A	74.1 ± 1.9	80.5 ± 1.5	85.9 ± 1.3	86.9 ± 1.2
P	90.5 ± 1.1	89.0 ± 1.2	89.3 ± 1.4	88.9 ± 1.4
R	78.9 ± 1.9	88.9 ± 1.6	95.5 ± 1.1	97.3 ± 1.1
S	38.4 ± 6.2	18.7 ± 4.2	13.9 ± 4.7	9.9 ± 3.5
F_1	84.3 ± 1.3	88.9 ± 0.9	92.3 ± 0.7	92.9 ± 0.7

However, some limitations of the methodology and algorithm implementation can be pointed out. For example, a number of false negatives (i.e. shots that the algorithm wrongly indicates that there is no X-ray emission) could be identified. More datasets may be needed for the algorithm to learn some of the unidentified features related to the hard X-ray emission. From the measurement point of view, there is a possibility that low intensity electric signals from the PMT were not detected by the oscilloscope, due to the signal-to-noise ratio at the instrument scale used. This can be explained considering that the vertical scale of the recording device was maintained at a constant value sufficiently high to enable the measurement of the highest intensity signals, without reaching the full scale. False positive shots were also found during the validation of the algorithm results. This is the case when the algorithm inferred from the antenna signal that there was an hard X-ray emission, but the PMT electric signal indicates the contrary. It is believed that there is still some over-fitting made by the algorithm.

IV. DISCUSSION

From the results presented above, it is clear that the emitted UHF signal has information, hidden in its complexity, about the conditions that were produced inside the plasma column that efficiently generate hard X-ray emissions.

There is a relationship, for a significant number of shots, between the radio-frequency measured with a Vivaldi antenna outside the vacuum chamber, and the hard X-ray emission detected with a Scintillator-Photomultiplier tube system. The use of an artificial intelligence algorithm proved to be necessary for handling the complexity of the signals. The algorithm found patterns in the antenna signals in terms of the standard deviation value of the Scintillator-PMT signal which allowed to detect the hard X-ray emission and, in a significant number of discharges, infer a standard deviation range value (R-value).

The binary classification using traditional machine learning algorithms presented similar results as the ones obtained using deep learning, in terms of the accuracy, recall and F_1 metrics (see Table 5). From this comparison, it is clear that different machine learning methods show consistency in supporting the conclusion about the relationship between the EM burst measurement and the hard X-ray detection.

Although the neural network showed that a relationship can be established between the UHF and hard X-ray radiation

measurements, the physical mechanisms that are responsible of this phenomena are still to be determined. In this work, the whole antenna signal is used as an input for the machine learning algorithm, which does not allow to determine the influence of the initial breakdown UHF emission with respect to the pinch phase emission in the presence of hard X-ray pulses. It is needed to deepen the understanding of the early physical processes [20] that determine the plasma column formation, and the UHF characterization of the pulsed plasma devices opens a new perspective to this analysis, including a more complete diagnostic that can include the electrical circuit oscillation into the study objects.

In order to comprehend the radiofrequency radiation emission from DPF devices, a detailed study on the discharge geometry is needed. Due to the compact design of the PF-400J, to be able to maintain the circuit impedance to the minimum, the origin of the radiofrequency emitted from the device cannot be traced back to a particular circuit element. Gerdin *et at.* [34] found that the parallel plates of the transmission line and capacitor bank of a DPF device were acting as antennas rather than waveguides. In the PF-400J, the entire device (electric circuit plus vacuum chamber) acts like an antenna, where the main EM transients detected with the Vivaldi antenna are those of the initial spark gap conduction, initial breakdown inside the vacuum chamber, pinch stage and column disruption (Fig. 3c). The plasma dynamics happening inside the device, that the antenna outside cannot measure, are believed to be indirectly responsible of the radiofrequency emitted outside the device and, because of this, it may be related in some way to the hard X-ray emission.

V. CONCLUSION

This work presents a novel diagnostic that enables the identification of hard X-ray emission from a pulsed plasma discharge, by analyzing the UHF electromagnetic radiation generated by the device, with machine learning techniques.

This diagnostic is based on the acquisition and analysis of the electromagnetic fields radiated from the electrical circuit that forms the discharge, at the moment of maximum column compression. These highly transient electric fields are responsible for the conditions for efficient electron acceleration towards the anode, and the generation of hard X-ray pulses.

The diagnostic presented in this work comprises the use of a low cost antenna design and artificial intelligence algorithms to relate the UHF emission with the hard X-ray pulse appearance during the normal operation of a transient current device. The capability to identify the presence of x-ray pulses with high certainty presents this diagnostic as a powerful and low cost tool to characterize pulsed plasma devices remotely, and without the need of high cost and complex detection systems for pulsed radiation.

REFERENCES

[1] M. G. Haines, "A review of the dense Z-pinch," *Plasma Phys. Controlled Fusion*, vol. 53, no. 9, 2011, Art. no. 093001. [Online]. Available: http://stacks.iop.org/0741-3335/53/i=9/a=093001

[2] C. Deeney *et al.*, "Power enhancement by increasing the initial array radius and wire number of tungsten Z pinches," *Phys. Rev. E, Stat. Phys. Plasmas Fluids Relat. Interdiscip. Top.*, vol. 56, no. 5, p. 5945, 1997.

[3] G. Avaria, M. Grisham, J. Li, F. G. Tomasel, V. N. Shlyaptsev, M. Busquet, M. Woolston, and J. J. Rocca, "Extreme degree of ionization in homogenous micro-capillary plasma columns heated by ultrafast current pulses," *Phys. Rev. Lett.*, vol. 114, Mar. 2015, Art. no. 095001. [Online]. Available: https://link.aps.org/doi/10.1103/PhysRevLett.114.095001

[4] D. H. Kalantar, D. A. Hammer, K. C. Mittal, N. Qi, F. C. Young, S. J. Stephanakis, P. G. Burkhalter, G. Mehlman, and D. A. Newman, "K-shell X-ray yield scaling for aluminum x-pinch plasmas," *J. Appl. Phys.*, vol. 73, no. 12, pp. 8134–8138, 1993. doi: 10.1063/1.353452.

[5] L. Soto, H. Chuaqui, M. Favre, and E. Wyndham, "Novel gas embedded compressional Z-pinch configuration," *Phys. Rev. Lett.*, vol. 72, no. 18, p. 2891, 1994.

[6] L. Soto, "New trends and future perspectives on plasma focus research," *Plasma Phys. Controlled Fusion*, vol. 47, no. 5A, p. A361, 2005. [Online]. Available: http://stacks.iop.org/0741-3335/47/i=5A/a=027

[7] P. Silva, J. Moreno, L. Soto, L. Birstein, R. E. Mayer, and W. Kies, "Neutron emission from a fast plasma focus of 400 joules," *Appl. Phys. Lett.*, vol. 83, no. 16, pp. 3269–3271, 2003. doi: 10.1063/1.1621460.

[8] L. Soto, P. Silva, J. Moreno, M. Zambra, W. Kies, R. E. Mayer, A. Clausse, L. Altamirano, C. Pavez, and L. Huerta, "Demonstration of neutron production in a table-top pinch plasma focus device operating at only tens of joules," *J. Phys. D, Appl. Phys.*, vol. 41, no. 20, 2008, Art. no. 205215.

[9] L. Soto, C. Pavéz, J. Moreno, L. Altamirano, L. Huerta, M. Barbaglia, A. Clausse, and R. E. Mayer, "Evidence of nuclear fusion neutrons in an extremely small plasma focus device operating at 0.1 joules," *Phys. Plasmas*, vol. 24, no. 8, 2017, Art. no. 082703.

[10] A. Tartaglione, R. Ramos, J. Gonzalez, A. Clausse, and C. Moreno, "Detection of water by neutron scattering using a small plasma focus," *Brazilian J. Phys.*, vol. 34, no. 4B, pp. 1756–1758, 2004.

[11] C. Pavez, J. Pedreros, M. Zambra, F. Veloso, J. Moreno, T.-S. Ariel, and L. Soto, "Potentiality of a small and fast dense plasma focus as hard X-ray source for radiographic applications," *Plasma Phys. Controlled Fusion*, vol. 54, no. 10, 2012, Art. no. 105018.

[12] J. L. Ellsworth, S. Falabella, V. Tang, A. Schmidt, G. Guethlein, S. Hawkins, and B. Rusnak, "Design and initial results from a kilojoule level dense plasma focus with hollow anode and cylindrically symmetric gas puff," *Rev. Sci. Instrum.*, vol. 85, no. 1, 2014, Art. no. 013504.

[13] L. Soto, C. Pavez, J. Moreno, M. J. Inestrosa-Izurieta, F. Veloso, G. Gutiérrez, J. Vergara, A. Clausse, H. Bruzzone, F. Castillo, and L. F. Delgado-Aparicio, "Characterization of the axial plasma shock in a table top plasma focus after the pinch and its possible application to testing materials for fusion reactors," *Phys. Plasmas*, vol. 21, no. 12, 2014, Art. no. 122703.

[14] C. Pavez, J. Pedreros, A. Tarifeño-Saldivia, and L. Soto, "Observation of plasma jets in a table top plasma focus discharge," *Phys. Plasmas*, vol. 22, no. 4, 2015, Art. no. 040705.

[15] M. J. Inestrosa-Izurieta, E. Ramos-Moore, and L. Soto, "Morphological and structural effects on tungsten targets produced by fusion plasma pulses from a table top plasma focus," *Nucl. Fusion*, vol. 55, no. 9, 2015, Art. no. 093011.

[16] R. S. Rawat, "High-energy-density pinch plasma: A unique nonconventional tool for plasma nanotechnology," *IEEE Trans. Plasma Sci.*, vol. 41, no. 4, pp. 701–715, Apr. 2013.

[17] M. J. Inestrosa-Izurieta, J. Moreno, S. Davis, and L. Soto, "Ti film deposition process of a plasma focus: Study by an experimental design," *AIP Adv.*, vol. 7, no. 10, 2017, Art. no. 105026. doi: 10.1063/1.4997877.

[18] J. Jain, J. Moreno, R. Andaur, R. Armisen, D. Morales, K. Marcelain, G. Avaria, B. Bora, S. Davis, C. Pavez, and L. Soto, "Hundred joules plasma focus device as a potential pulsed source for *in vitro* cancer cell irradiation," *AIP Adv.*, vol. 7, no. 8, 2017, Art. no. 085121. doi: 10.1063/1.4994655.

[19] L. Soto, C. Pavez, A. Tarifeño, J. Moreno, and F. Veloso, "Studies on scalability and scaling laws for the plasma focus: Similarities and differences in devices from 1 MJ to 0.1 J," *Plasma Sources Sci. Technol.*, vol. 19, no. 5, 2010, Art. no. 055017. [Online]. Available: http://stacks.iop.org/0963-0252/19/i=5/a=055017

[20] A. Bernard, H. Bruzzone, P. Choi, H. Chuaqui, V. Gribkov, J. Herrera, K. Hirano, A. Krejci, S. Lee, C. Luo, F. Mezzetti, M. J. Sadowski, H. Schmidt, K. Ware, C. S. Wong, and V. Zoita, "Scientific status of plasma focus research," *J.-Moscow Phys. Soc.*, vol. 8, pp. 93–170, Nov. 1998.

[21] M. Zambra, P. Silva, C. Pavez, D. Pasten, J. Moreno, and L. Soto, "Experimental results on hard X-ray energy emitted by a low-energy plasma focus device: A radiographic image analysis," *Plasma Phys. Controlled Fusion*, vol. 51, no. 12, 2009, Art. no. 125003. [Online]. Available: http://stacks.iop.org/0741-3335/51/i=12/a=125003

[22] J. Jain, J. Moreno, R. E. Avila, G. Avaria, C. Pavez, B. Bora, S. Davis, and L. Soto, "Pulsed X-rays dose measurements from a hundred joules plasma focus device," *J. Phys., Conf. Ser.*, vol. 1043, no. 1, 2018, Art. no. 012048. [Online]. Available: http://stacks.iop.org/1742-6596/1043/i=1/a=012048

[23] J. W. Mather, "15. Dense plasma focus," in *Methods in Experimental Physics*, vol. 9. Amsterdam, The Netherlands: Elsevier, 1971, pp. 187–249.

[24] L. Soto, C. Pavez, J. Moreno, M. Cárdenas, A. Tarifeño, P. Silva, M. Zambra, L. Huerta, C. Tenreiro, J. L. Giordano, M. Lagos, C. Retamal, R. Escobar, J. Ramos, and L. Altamirano, "Dense transient pinches and pulsed power technology: Research and applications using medium and small devices," *Phys. Scripta*, vol. 2008, no. T131, 2008, Art. no. 014031.

[25] J. Moreno, F. Veloso, C. Pavez, A. Tarifeño-Saldivia, D. Klir, and L. Soto, "Neutron energy distribution and temporal correlations with hard X-ray emission from a hundreds of joules plasma focus device," *Plasma Phys. Controlled Fusion*, vol. 57, no. 3, 2015, Art. no. 035008.

[26] D. D. Ryutov, M. S. Derzon, and M. K. Matzen, "The physics of fast Z pinches," *Rev. Mod. Phys.*, vol. 72, no. 1, p. 167, Jan. 2000.

[27] K. Schönbach, L. Michel, and H. Fischer, "Correlation of soft X-ray spots with hard radiation and neutron emission in a 1-kJ plasma focus," *Appl. Phys. Lett.*, vol. 25, no. 10, pp. 547–549, 1974.

[28] P. Choi, C. S. Wong, and H. Herold, "Studies of the spatial and temporal evolution of a dense plasma focus in the X-ray region," *Laser Part. Beams*, vol. 7, no. 4, pp. 763–772, 1989.

[29] I. Escalona, G. Avaria, M. Díaz, J. Ardila-Rey, J. Moreno, C. Pavez, and L. Soto, "Electromagnetic burst measurement system based on low cost uhf dipole antenna," *Energies*, vol. 10, no. 9, p. 1415, 2017.

[30] C. Balanis, *Antenna Theory: Analysis and Design*, no. 1. Hoboken, NJ, USA: Wiley, 2005.

[31] P. J. Gibson, "The vivaldi aerial," in *Proc. 9th Eur. Microw. Conf.*, Sep. 1979, pp. 101–105.

[32] G. Robles, R. Albarracín, J. Vázquez-Roy, E. Rajo-Iglesias, J. M. Martínez-Tarifa, M. V. Rojas-Moreno, M. Sánchez-Fernández, and J. Ardila-Rey, "On the use of vivaldi antennas in the detection of partial discharges," in *Proc. IEEE Int. Conf. Solid Dielectr. (ICSD)*, Jun./Jul. 2013, pp. 302–305.

[33] A. Schmidt, A. Link, D. Welch, J. Ellsworth, S. Falabella, and V. Tang, "Comparisons of dense-plasma-focus kinetic simulations with experimental measurements," *Phys. Rev. E, Stat. Phys. Plasmas Fluids Relat. Interdiscip. Top.*, vol. 89, no. 6, 2014, Art. no. 061101.

[34] G. Gerdin, M. J. Tanis, and F. Venneri, "Observation of microwave emission from a plasma focus at frequencies well below the mean plasma frequency," *Plasma Phys. Controlled Fusion*, vol. 28, no. 3, p. 527, 1986.

[35] D. Piriaei, T. D. Mahabadi, S. Javadi, and M. Ghoranneviss, "The effects of the cathode array on emitted hard X-ray from a small plasma focus device," *Phys. Plasmas*, vol. 24, no. 8, 2017, Art. no. 083508.

[36] Y. LeCun, Y. Bengio, and G. Hinton, "Deep learning," *Nature*, vol. 521, no. 7553, p. 436, 2015.

[37] K. Xu, J. Ba, R. Kiros, K. Cho, A. Courville, R. Salakhudinov, R. Zemel, and Y. Bengio, "Show, attend and tell: Neural image caption generation with visual attention," in *Proc. Int. Conf. Mach. Learn.*, 2015, pp. 2048–2057.

[38] T. Young, D. Hazarika, S. Poria, and E. Cambria, "Recent trends in deep learning based natural language processing," *IEEE Comput. Intell. Mag.*, vol. 13, no. 3, pp. 55–75, Aug. 2018.

[39] S. Ö. Arik, M. Chrzanowski, A. Coates, G. Diamos, A. Gibiansky, Y. Kang, X. Li, J. Miller, A. Ng, J. Raiman, S. Sengupta, and M. Shoeybi, "Deep voice: Real-time neural text-to-speech," in *Proc. 34th Int. Conf. Mach. Learn.*, vol. 70, 2017, pp. 195–204.

[40] D. Silver, A. Huang, C. J. Maddison, A. Guez, L. Sifre, G. van den Driessche, J. Schrittwieser, I. Antonoglou, V. Panneershelvam, M. Lanctot, S. Dieleman, D. Grewe, J. Nham, N. Kalchbrenner, I. Sutskever, T. Lillicrap, M. Leach, K. Kavukcuoglu, T. Graepel, and D. Hassabis, "Mastering the game of go with deep neural networks and tree search," *Nature*, vol. 529, no. 7587, pp. 484–489, 2016.

[41] D. Silver, J. Schrittwieser, K. Simonyan, I. Antonoglou, A. Huang, A. Guez, T. Hubert, L. Baker, M. Lai, A. Bolton, Y. Chen, T. Lillicrap, F. Hui, L. Sifre, G. van den Driessche, T. Graepel, and D. Hassabis, "Mastering the game of go without human knowledge," *Nature*, vol. 550, no. 7676, pp. 354–359, 2017.

[42] B. K. Spears, J. Brase, P.-T. Bremer, B. Chen, J. Field, J. Gaffney, M. Kruse, S. Langer, K. Lewis, R. Nora, J. L. Peterson, J. J. Thiagarajan, B. Van Essen, and K. Humbird, "Deep learning: A guide for practitioners in the physical sciences," *Phys. Plasmas*, vol. 25, no. 8, Aug. 2018, Art. no. 080901. [Online]. Available: http://aip.scitation.org/doi/10.1063/1.5020791

[43] J. Kates-Harbeck, A. Svyatkovskiy, and W. Tang, "Predicting disruptive instabilities in controlled fusion plasmas through deep learning," *Nature*, vol. 568, pp. 526–531, Apr. 2019. [Online]. Available: http://www.nature.com/articles/s41586-019-1116-4

[44] D. G. Pellinen, M. S. Di Capua, S. E. Sampayan, H. Gerbracht, and M. Wang, "Rogowski coil for measuring fast, high-level pulsed currents," *Rev. Sci. Instrum.*, vol. 51, no. 11, pp. 1535–1540, 1980.

[45] A. Schwab, *High-Voltage Measurement Techniques* (Monographs in Modern Electrical Technology). Cambridge, MA, USA: MIT Press, 1972.

[46] W. L. Stutzman and G. A. Thiele, *Antenna Theory Design*. Hoboken, NJ, USA: Wiley, 2012.

[47] R. E. Collin, *Antennas and Radiowave Propagation*. New York, NY, USA: McGraw-Hill, 1985.

[48] R. Albarracín, G. Robles, J. M. Martinez-Tarifa, and J. Ardila-Rey, "Separation of sources in radiofrequency measurements of partial discharges using time–power ratio maps," *ISA Trans.*, vol. 58, pp. 389–397, Sep. 2015.

[49] G. Robles, J. M. Fresno, J. M. Martínez-Tarifa, J. A. Ardila-Rey, and E. Parrado-Hernández, "Partial discharge spectral characterization in HF, VHF and UHF bands using particle swarm optimization," *Sensors*, vol. 18, no. 3, p. 746, 2018.

[50] F. Chollet. (2015). *Keras*. [Online]. Available: https://keras.io

[51] M. Sokolova and G. Lapalme, "A systematic analysis of performance measures for classification tasks," *Inf. Process. Manage.*, vol. 45, no. 4, pp. 427–437, 2009.

GONZALO AVARIA was born in Concepción, Chile in 1980. He received the B.Sc. degree in physics from the Universidad de Concepción, Concepción, in 2002, and the Ph.D. degree in physics from the Pontificia Universidad Católica de Chile, Santiago, Chile, in 2008. From 2009 to 2011, he was a Postdoctoral Fellow with the NSF Engineering Research Center for Extreme Ultraviolet Science and Technology, Colorado State University, Fort Collins, CO, USA. Since 2011, he has been a Researcher with the Nuclear Sciences Department, Chilean Nuclear Energy Commission, Santiago. His current research interests include plasma spectroscopy, dense transient plasmas, pulsed capillary discharges, plasma focus discharges, and transient plasma diagnostics. Dr. Avaria is a member of the American Physical Society and the Chilean Physical Society. He was a recipient of the Universidad de Concepción Award for Outstanding Students in 2002.

JORGE ARDILA-REY was born in Santander, Colombia, in 1984. He received the B.Sc. degree in mechatronic engineering from the Universidad de Pamplona, Pamplona, Colombia, in 2007, the Specialist Officer degree in naval engineering from Escuela Naval Almirante Padilla, Cartagena, Colombia, in 2008, and the M.Sc. and Ph.D. degrees in electrical engineering from the Universidad Carlos III de Madrid (UC3M), in 2012 and 2014, respectively. He was an Automatic Control Engineer with ARC Almirante Padilla, from 2008 to 2010.

From 2010 to 2014, he was with the Department of Electrical Engineering and the High-Voltage Research and Test Laboratory (LINEALT), UC3M. He is currently a Professor with the Department of Electrical Engineering, Universidad Técnica Federico Santa María, Santiago, Chile. His research interests include partial discharges, insulation systems diagnosis and instrumentation, and measurement techniques for high frequency currents.

SERGIO DAVIS was born in Santiago, Chile, in 1978. He received the B.Sc. degree in applied physics and the physics engineer title from the Universidad de Santiago, Santiago, Chile, in 2003, and the Ph.D. degree in applied materials physics from the Royal Institute of Technology (Kungliga Tekniska Högskolan, KTH), Stockholm, Sweden, in 2009. From 2011 to 2015, he was an Assistant Professor with the Facultad de Ciencias, Universidad de Chile, Santiago. He has been an Adjunct Associate Professor with Universidad Andrés Bello, Santiago, since 2017. He is currently a Researcher of theoretical physics with the Department of Nuclear Sciences, Chilean Nuclear Energy Commission (CCHEN). His research interests include nonequilibrium statistical physics, plasma physics, metastable states at the onset of phase transitions, stochastic computer simulation methods, and Bayesian probability/maximum entropy formalisms.

LUIS ORELLANA was born in San Fernando, Chile, in 1992. He received the B.S. degree in electrical engineering from Federico Santa Maria Technical University, in 2015, where he is currently pursuing the M.S. degree in electrical engineering.

Since 2018, he has been working on the thesis about the relationship between the electromagnetic burst from dense plasma focus and other diagnostics of the device with the Plasma and Nuclear Fusion Laboratory, Chilean Nuclear Energy Commission. His research interests include the application of high voltage techniques to pulsed power devices and signal analysis.

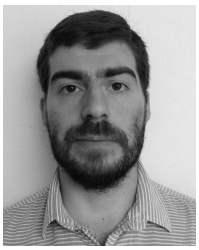

BENJAMÍN CEVALLOS was born in Puerto Varas, Chile, in 1991. He received the B.Sc. degree in electrical engineering and the Engineering degree from Federico Santa María Technical University (USM), where he has been working on the thesis related to measurements of high voltage phenomena. His research interest includes the application of high voltage techniques for data acquisition.

CRISTIAN PAVEZ was born in Santiago, Chile, in 1972. He received the B.S. and M.S. degrees in physics from the Pontificia Universidad Católica de Chile, Santiago, in 1998 and 2005, respectively, and the Ph.D. degree from the University of Concepción, Concepción, Chile, in 2007, developing his Ph.D. thesis in experimental plasma physics with the Plasma Physics and Nuclear Fusion Laboratory, Nuclear Chilean Energy Commission (CCHEN). Since 2008, he has been with the CCHEN Plasma Group as a Researcher, and an Adjunct Associate Researcher of the Ph.D. Program in physics with Physical Sciences Department, Universidad Andres Bello, Chile, since 2016. His current research interests include dense transient plasmas, including Z-pinch, plasma focus and capillary discharges, transient plasma diagnostics, optical and digital holography, optical and digital interferometry and optical refractive diagnostics. He is a member of the Optical Society (OSA) and the Chilean Physical Society (SOCHIFI).

LEOPOLDO SOTO received the B.S., M.S., and Ph.D. degrees in physics from the Pontificia Universidad Católica de Chile, Santiago, in 1989, 1990, and 1993, respectively. His current research interests include dense transient plasmas, pulsed power and applied optics, including Z-pinch, plasma focus, nuclear fusion mechanisms, capillary discharges, pulsed power miniature devices, effects of pulsed radiation on materials and on biological objects, transient plasma diagnostics, holography, and interferometry and optical refractive diagnostics.

He is an Associate Professor of the Ph.D. Program in physics with the University of Concepción, Chile, and the Ph.D. Program in applied science with the University of Talca, Chile. He is currently the Head of the Plasma Physics and Nuclear Fusion Laboratory, Nuclear Chilean Energy Commission (CCHEN), and the Director of the Center for Research and Applications in Plasma Physics and Pulsed Power, P4. He is an Associate Full Professor with the Physical Sciences Department, Universidad Andres Bello, Chile. In 2007, he was elected as a Fellow of the Institute of Physics, U.K. In 1999, he received the Presidential Chair in Science by the President of Chile.

He was the President of the Chilean Physical Society (SOCHIFI), for 2 periods, from 2003 to 2008, and the Secretary General of Chilean Physical Society (SOCHIFI), from 2017 to 2019. Since 2017, he has been a Scientific Advisory of the Commission of Challenges of the Future, Science, Technology and Innovation of the Senate of the Republic of Chile.